Journal of Organometallic Chemistry 694 (2009) 1922–1928

Contents lists available at ScienceDirect

Journal of Organometallic Chemistry

journal homepage: www.elsevier.com/locate/jorganchem

Four-coordinate boron compounds derived from 2-(2-pyridyl)phenol ligand as novel hole-blocking materials for phosphorescent OLEDs

Nam Gwang Kim, Chang Hwan Shin, Min Hyung Lee *, Youngkyu Do *

Department of Chemistry, School of Molecular Science BK-21, KAIST, Daejeon 305-701, Republic of Korea

ARTICLE INFO

Article history:
Received 28 October 2008
Received in revised form 15 January 2009
Accepted 20 January 2009
Available online 24 January 2009

Keywords:
Four-coordinate boron
2-(2-Pyridyl)phenol
Hole-blocking material
Organic light-emitting diode
Phosphorescence

ABSTRACT

Four-coordinate boron compounds of $Ph_2B \cdot$ **1** (**2**) and $(C_6F_5)_3B$(**1** · H) (**3**) were prepared from the reaction of 2-(2-pyridyl)phenol (**1** · H) ligand with triarylborane starting materials, BPh_3 and $B(C_6F_5)_3$, respectively, and tested as hole-blocking layer (HBL) materials in phosphorescent OLEDs. While the crystal structure of **2** reveals the pseudo-tetrahedral geometry around the boron center with bidentate [*N*,*O*] chelation by **1**, **3** is characterized as the zwitterionic four-coordinate system where the ligand **1** · H acts as monodentate [*O*] chelator with *N*-protonation. UV–Vis absorption and PL spectra of **2** and **3** are consistent with the ligand-centered, HOMO–LUMO electronic transitions with charge transfer from a phenoxide ring to a pyridine, which was further supported by time dependent DFT calculation for **2**. Both compounds are found to possess the HOMO–LUMO energy gap of 3.1 eV appropriate for hole-blocking materials for phosphorescent OLEDs. The devices incorporating **2** and **3** as HBL materials displayed stable green phosphorescence of $Ir(ppy)_3$ (ppy = 2-phenylpyridine) with low turn-on voltage of 3.2 and 3.4 V, respectively, indicating that **2** and **3** function as HBL materials. Although both devices show the short lifetime (<1 h) probably owing to the low thermal stability, the device based on **2** displays better performances in terms of luminance, power and luminance efficiency, and external quantum efficiency in a wide range of current densities (0.1–100 mA/cm^2) than the reference device incorporating BAlq as HBL materials.

1. Introduction

Organic light-emitting devices (OLEDs) based on phosphorescent emitters that have attracted great interest due to high internal quantum efficiency, up to 100% of a theoretical value [1], have raised new demand for the development of hole-blocking materials in order to confine triplet excitons in the emitting layer (EML) and thereby achieving high efficiency [2,3]. Various organic and organometallic compounds have been introduced as the hole-blocking layer (HBL) [2–9] or the electron-transporting layer with hole-blocking ability (HBETL) [5,6]. Among them, 2,9-dimethyl-4,7-diphenyl-1,10-phenanthroline, known as bathocuproine (BCP) [3], and bis(2-methyl-8-quinolinolato)-mono(4-phenylphenolato)-aluminium (BAlq) [5,7] are known as typical HBL materials. Candidates for such HBL materials are generally required to have good electron transporting ability and an energy level of lowest unoccupied molecular orbital (LUMO) comparable to those of the adjacent electron transporting and emitting layer materials. Most importantly, they should have a wide energy gap with an energy level of highest occupied molecular orbital (HOMO) lower than that of the emitting layer to block holes from overflowing from the emitting layer into the electron transporting layer (ETL) and to prevent the diffusion of triplet excitons that may lead to thermal quenching or emissive contamination [8].

In order to develop novel HBL materials to meet these criteria, our group has been interested in the group 13 compounds supported by multidentate chelating ligand and recently demonstrated that the Al complexes based on tetradentate salen ligand can serve as efficient HBL materials for phosphorescent OLEDs [9]. As part of these efforts, we also devoted our attention to four-coordinate boron compound particularly possessing [*N*,*O*] chelating ligand. Although boron compounds such as triarylborane (BAr_3) have been successfully employed as efficient HBL materials due to their electron deficient nature and thereby good electron transporting ability [8], there is no reported example of mononuclear four-coordinate boron compounds as hole-blocking materials. Instead, boron compounds bearing [*N*,*O*] bidentate heterocyclic ligand such as Ar_2Bq (q = 8-quinolinolato) have actively been investigated as EML or ETL materials in OLEDs [10]. However, such compounds based on 8-hydroxyquinoline ligand could be less suitable for hole-blocking materials owing to a small HOMO–LUMO energy band gap (2.7 eV) [11], as also indicated by their green fluorescence. Since the energy band gap of the four-coordinate Ar_2B[*N*,*O*] type compounds are mainly characterized by the [*N*,*O*] chelating ligand, it would be desired to search for a wide

* Corresponding authors. Tel.: +82 42 350 2829; fax: +82 42 350 2810 (Y. Do).
E-mail addresses: lmh74@kaist.ac.kr (M.H. Lee), ykdo@kaist.ac.kr (Y. Do).

0022-328X/$ - see front matter © 2009 Elsevier B.V. All rights reserved.
doi:10.1016/j.jorganchem.2009.01.035

band gap [*N*,*O*] ligand for efficient HBL materials. To this end, we focused on 2-(2-pyridyl)phenol as a new bidentate [*N*,*O*] ligand since it has a wide band gap of theoretical value of ca. 4.0 eV [12] and contains pyridine and phenolate rings to coordinate bidentatedly with a boron center. Furthermore, the previous reports showed that Be [13,14], Al [15], and Zn [16] complexes of 2-(2-pyridyl)phenolate have a large energy band gap enough to be used as blue or violet-blue emitting materials, which may thus render the four-coordinate boron compound based on 2-(2-pyridyl)phenol appropriate for potential HBL materials.

In this report, the synthesis, structure, and OLED characteristics of boron compounds derived from 2-(2-pyridyl)phenol ligand as the first example of hole-blocking materials based on four-coordinate boron compound are described.

2. Result and discussion

2.1. Synthesis and characterizations

As shown in Scheme 1, reaction of 2-(2-pyridyl)phenol (**1** · H) [12] with triphenylborane (BPh_3) in refluxing tetrahydrofuran (THF) produced the four-coordinate boron compound **2** with bidentate [*N*,*O*] chelation by **1** as ivory powder in good yield (70%). In order to explore the electronic effect of an aryl group, pentafluorophenyl substituted borane ($B(C_6F_5)_3$) was introduced as a reactant with an expectation that the electron-withdrawing effect of C_6F_5 group may increase the Lewis acidity of the boron center and thereby affect HOMO and LUMO energy levels. Interestingly, it was found that the reaction of $B(C_6F_5)_3$ with **1** · H in refluxing THF solely produces the zwitterionic four-coordinate **3** where the ligand **1** · H acts as monodentate [*O*] chelator with *N*-protonation (*vide infra*). Extended heating or change of the solvent to benzene didn't induce any formation of the expected [*N*,*O*] chelated structure. Although the [*O*] chelation with *N*-protonation by **1** · H is similar to that found in the reaction of $B(C_6F_5)_3$ with 8-hydroxyquinoline [17], it is reported that the heating of the reaction mixture finally afforded the [*N*,*O*] chelated $(C_6F_5)_2Bq$ compound in the latter system. The compounds **2** and **3** have been fully characterized by multinuclear NMR spectroscopy (^1H, ^{13}C, ^{11}B, and ^{19}F NMR) and elemental analysis. While the ^{11}B NMR signals detected at δ = 5.7 and −2.4 ppm for **2** and **3**, respectively, confirm the presence of a four-coordinate boron center, the upfield shift of the boron resonance for **3** further supports the zwitterionic nature of **3**, as similarly observed in the 8-hydroxyquinoline adduct $(C_6F_5)_3B(qH)$ (−3.1 ppm). In contrast, the boron signal of **2** at 5.7 ppm is in the similar range reported for the Ar_2Bq (11.1 ppm for Ar = Ph; 7.0 ppm for Ar = C_6F_5) compounds, thus pointing to the [*N*,*O*] chelation of boron center in **2** [17]. The ^1H NMR spectrum of **3** also clearly exhibits the proton resonance at δ = 16.6 ppm, revealing the formation of zwitterionic species through the *N*-protonation of pyridyl group. In agreement with the different structural features observed for **2** and **3**, the thermal stability determined by TGA measurements is found to be higher for the structurally rigid **2** (T_{d5} = 268 °C) than for **3** (T_{d5} = 201 °C), both of which, however, are in the range of relatively low thermal stability.

The crystal structures of **2** and **3** were determined by single crystal X-ray diffraction study. As shown in Fig. 1, **2** exhibits the four-coordinate structure with bidentate [*N*,*O*] chelation by **1** to the boron atom, as consistent with its ^{11}B NMR signal. The O–B–N, O–B–C13, and O–B–C19 angles and the sum of these angles of 324.7° around the boron center in **2** is rather deviated from the ideal values of 109.5° and 328.5°, respectively, for the tetrahedral geometry, indicating the pseudo-tetrahedral geometry around the boron center. The latter angle is also larger than those observed in Ph_2Bq (314.8° for molecule I and 317.7° for molecule II)[18] and $(C_6F_5)_2Bq$ (319.6°) [17]. This finding could be mainly attributed to the increased O–B–N bite angle in **2** (104.97(15)°) by ca. 8.4° and 5.5°, respectively, when compared to those in Ph_2Bq (96.6(7)° for molecule I and 96.7(8)° for molecule II) [18] and $(C_6F_5)_2Bq$ (99.43(13)°) [17], probably owing to the six-membered ring nature of **1**. While the B–O bond length of 1.480(2) Å in **2** is shorter than that in Ph_2Bq (1.56(1) Å), the B–C and B–N bonds are slightly lengthened in comparison with those in Ph_2Bq within 0.02 Å [18]. It is interesting to note that the phenolate and pyridine rings of 2-(2-pyridyl)phenolate moiety in **2** are distorted to form a dihedral angle (θ) of 20°. This angle is larger than that observed in $Be(\mathbf{1})_2$ (11°) [14] and quite similar to the calculated angle of the free ligand **1**·H (21.53°) [19]. Moreover, the bidentate coordination of **1** with the boron center may endow 2-(2-pyridyl)phenolate moiety with stronger rigidity in comparison with free **1** · H, which may lead to reduction of the loss of energy via vibrational motions and thereby increase emission efficiency [14,19].

In the crystal structure of **3**, it can be seen that the **1** · H ligand adopts *O*-coordination mode to the boron center, as confirmed by the spectroscopic data (Fig. 2). The sum of C_{Ar}–B–C_{Ar} angles of 332.7° in **3** is almost comparable to that observed in $(C_6F_5)_3B(qH)$ (332.3°), indicating the disorted tetrahedral geometry around the

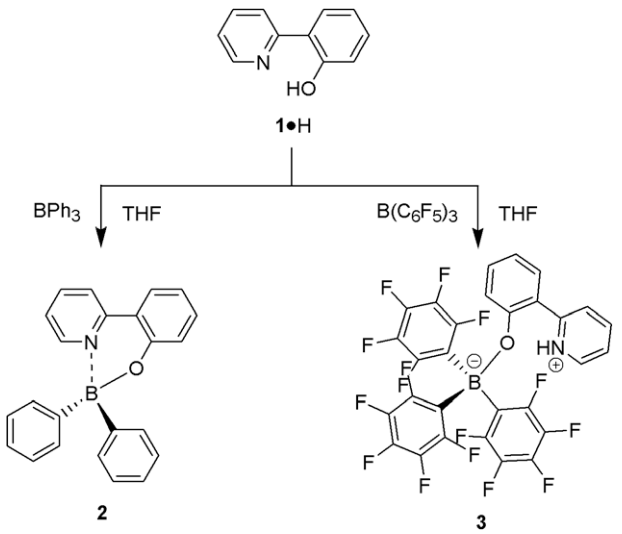

Scheme 1.

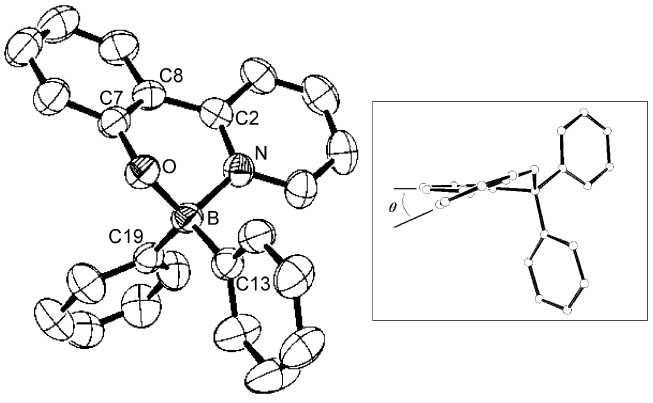

Fig. 1. Molecular structure of compound **2** (50% thermal ellipsoid). Hydrogen atoms are omitted for clarity. Selected bond distances (Å) and angles (°): O–C7 1.351(2), N–C6 1.346(2), B–N 1.627(2), B–O 1.480(2), B–C13 1.616(3), B–C19 1.607(3), N–C2–C8 117.96(18), C2–C8–C7 119.41(18), C8–C7–O 120.38(19), O–B–N 104.97(15), N–B–C13 109.28(16), N–B–C19 107.20(17), O–B–C13 106.90(18), O–B–C19 112.84(17), C13–B–C19 115.15(16). Inset: dihedral angle (θ) between the pyridine and phenolate planes.

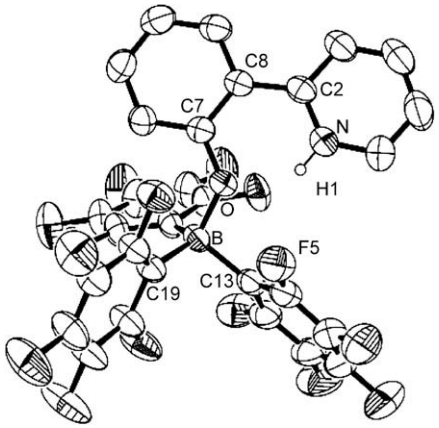

Fig. 2. Molecular structure of compound **3** (35% thermal ellipsoid). Hydrogen atoms are omitted for clarity. Selected bond distances (Å) and angles (°): O–C7 1.359(3), N–C6 1.341(4), B–O 1.520(3), B–C13 1.657(4), B–C19 1.647(4), B–C25 1.643(4), N–C2–C8 119.1(2), C2–C8–C7 123.0(2), C8–C7–O 118.2(2), O–B–C25 107.2(2), C25–B–C13 112.7(2), C25–B–C19 114.9(2), O–B–C13 104.0(2), O–B–C19 112.6(2), C13–B–C19 105.1(2), C7–O–B 126.6(2)°.

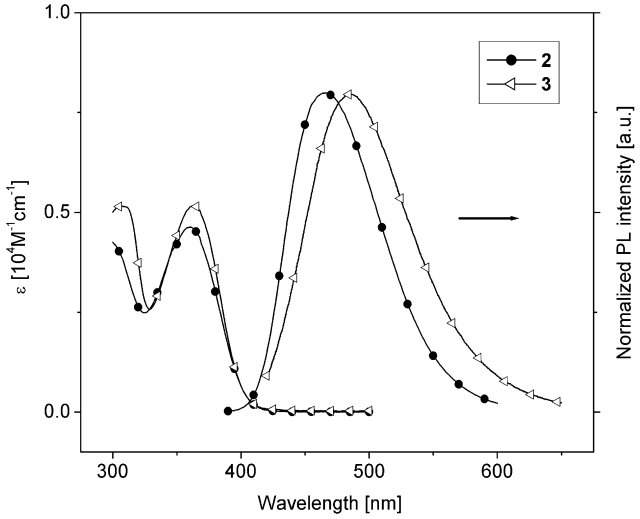

Fig. 3. UV–Vis absorption and photoluminescence (PL) spectra of **2** and **3**.

boron center [17]. Although the slightly longer B–O bond length of 1.520(2) Å and the shorter B–C bond lengths (1.643(4)–1.657(4) Å) are observed for **3** in comparison with those reported in $(C_6F_5)_3B(qH)$ (1.508(4) Å and 1.654(5)–1.664(4) Å, respectively) [17], the differences are not appreciable. Similarly, the C7–O–B bond angle of 126.6(2)° is in good agreement with that in $(C_6F_5)_3B(qH)$ (126.8(2)°). All these structural features for **3** reflect the resemblance of boron coordination sphere in **3** with the 8-hydroxyquinoline adduct $(C_6F_5)_3B(qH)$. It seems that there exists no hydrogen bonding interaction between the N–H proton and the nearby fluorine atom (F5), as judged by the long N–H···F distance of 2.66 Å.

2.2. UV–Vis and photoluminescence (PL) spectroscopy

UV–Vis absorption and PL spectra of compounds **2** and **3** are measured in chloroform (Fig. 3 and Table 1). Compounds **2** and **3** exhibit the similar absorption bands with a slightly red-shifted absorption maximum for **3** (360 nm and 363 nm for **2** and **3**, respectively) despite the structural difference. These absorption features of **2** and **3** are similar with those of free ligand **1** · H as well as Be [13,14] and Zn [16] complexes containing **1**, suggesting that the electronic transitions in **2** and **3** are ligand-centered π–π^* transitions (*vide infra*). Both **2** and **3** exhibit bright sky blue luminescence with high quantum efficiencies in solution. While the emission maximum wavelengths are rather different from each other in solution, showing 20 nm red-shift for **3** (465 nm and 485 nm for **2** and **3**, respectively), the PL spectra of the vacuum deposited film of both compounds are quite similar (Fig. S3 in Supplementary material). This result could be related to the loss of energy in the excited state via vibrational motions due to the flexible nature of ligand in the monodentate adduct **3** in solution.

The cyclic voltammetry measurements show that both compounds **2** and **3** undergo irreversible oxidation process and the HOMO energy levels of **2** and **3** are determined to be 5.4 and 5.5 eV from the oxidation onset potential, respectively [20]. The HOMO–LUMO energy gap of **2** and **3** estimated from the absorption edges of the optical absorption spectra is almost identical with each other, affording ca. 3.1 eV (Table 1). The equally lower HOMO and LUMO energy levels for **3** than those for **2** by 0.1 eV might be attributed to the stabilization of HOMO (phenolate ring) and LUMO (pyridine ring) by the positive charge developed on the ligand upon *N*-protonation.

Table 1
Photophysical properties and energy levels for compounds **2** and **3**.

Compounds	λ_{abs}[a] (nm) ($\log\varepsilon$)	λ_{em}[a] (nm) (Φ)[b]/ solution	λ_{em} (nm)/ film	HOMO[c] (eV)	LUMO[d] [eV]
2	360 (3.67)	465 (0.40)	464	5.4	2.3
3	363 (3.73)	485 (0.25)	469	5.5	2.4

[a] In chloroform solution (1.0×10^{-5} M).
[b] Quinine sulfate ($\Phi = 0.55$) used as a standard [21].
[c] Determined from the oxidation onset potentials measured by cyclic voltammetry in CH_2Cl_2 [20].
[d] Estimated from the HOMO level and the absorption edge.

2.3. Computational study on **2**

To gain insight into the electronic transition and the HOMO-LUMO energy levels, time dependent-DFT (TD-DFT) calculations have been carried on geometry of **2** optimized from the X-ray structure at the B3LYP [22]/6-31G(d) [23] level. The optimized geometry and molecular orbitals for the ground state of **2** are displayed in Fig. 4. The calculation results show that the transition from HOMO to LUMO has the largest contribution to the low-energy electronic transition (Table S1 in Supplementary material). It can also be seen that the delocalized electron density of HOMO is mainly located on the phenoxide ring with an orbital contribution of 73% while LUMO is localized on the pyridyl ring (77%). This finding suggests that the low-energy electronic transition would occur predominantly through ligand-centered π–π^* transitions with charge transfer from a phenoxide ring to a pyridine. In fact, these features are very similar to those observed in the free **1** · H and Be complexes [19], as well as in the 8-hydroxyquinoline-based boron compounds (Ar_2Bq) [17]. Although the calculated absorption maximum wavelength of 387 nm is rather shifted toward lower energy than the experimental wavelength (360 nm), it was revealed that when the solvation effect of chloroform is included using the polarized continuum model (PCM) [24], the calculated wavelength (372 nm) becomes comparable to the experimental value.

2.4. Hole-blocking properties in OLEDs

Since the optical properties and HOMO–LUMO energy levels of **3** are similar to those of **2**, both compounds **2** and **3** were introduced as a hole-blocking material for phosphorescent OLEDs based

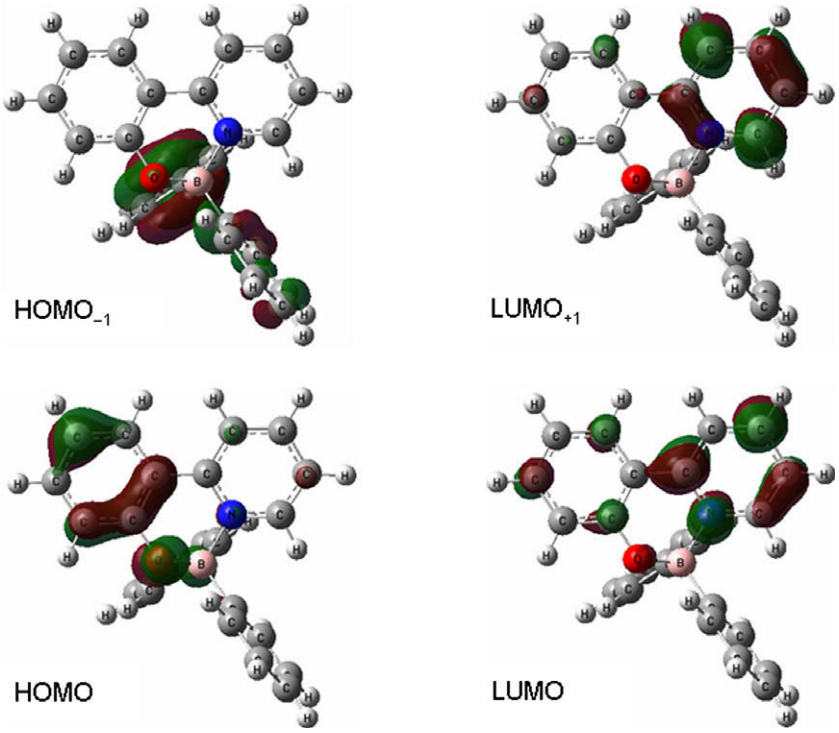

Fig. 4. Optimized geometry and frontier molecular orbital diagrams of **2** from B3LYP calculations (isovalue = 0.05 a.u.).

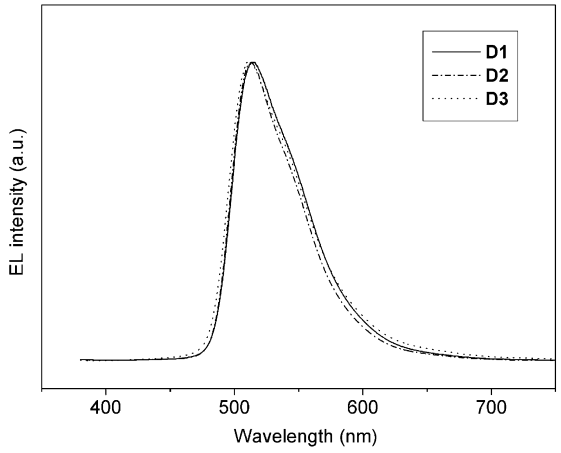

Fig. 5. Electroluminescent spectra of devices **D1**, **D2**, and **D3**.

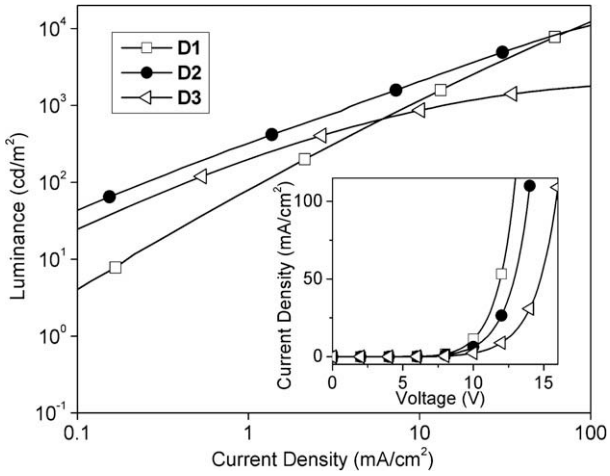

Fig. 6. Luminance vs. current density characteristics of devices **D1**, **D2**, and **D3**. Inset: Current density vs. voltage characteristics of the devices.

on *fac*-tris(2-phenylpyridinato)iridium(III) ($Ir(ppy)_3$) emitter. Moreover, based on the observation that the film PL spectrum of **3** is comparable to that in solution as well as that of **2**, we note that **3** is able to form a stable vacuum sublimated film despite its zwitterionic nature. In order to compare the performance of the devices, BAlq [3], which is well-known and commonly used hole-blocking material, was selected for control HBL material. Each device was fabricated with the following structure: ITO/CuPc (10 nm)/α-NPD (30 nm)/CBP:$Ir(ppy)_3$ (8 wt%) (30 nm)/**HBL** (10 nm)/Alq_3 (30 nm)/LiF (1 nm)/Al (100 nm) (**HBL** = BAlq (**D1**), **2** (**D2**), **3** (**D3**); CuPc = copper phthalocyanine; α-NPD = 4,4′-bis(1-naphthylphenylamino)biphenyl; CBP = 4,4′-bis(*N*-carbazolyl)-biphenyl).

All the devices exhibit green phosphorescence originated from $Ir(ppy)_3$ with the emission maxima at 515 nm, and there is no emissive contamination due to other materials at any condition of current density (Fig. 5). **D3** maintained the CIE color coordinate at (0.27, 0.62) as the current density increased from 10 mA/cm^2 to 100 mA/cm^2. In the case of **D1** and **D2**, the CIE color coordinate was slightly changed from (0.27, 0.64) and (0.26, 0.64) to (0.27, 0.63) and (0.26, 0.63), respectively. These results clearly indicate that **2** and **3** function properly as HBL materials.

The current density–voltage–luminance (*J*–*V*–*L*) characteristics for the devices are illustrated in Fig. 6 and the key parameters of the device performance are summarized in Table 2. The devices **D2** and **D3** exhibit lower turn-on voltages of 3.2 V and 3.4 V, respectively, compared to that of **D1** (4.6 V), indicating facile electron injection into the emitting layer in **D2** and **D3**.

While the current density of **D1** increases faster than **D2** with increasing applied voltage, **D2** exhibits higher luminance than **D1** over a wide range of current density range (0.1–100 mA/cm^2)

Table 2
Electroluminescent performance characteristics of **D1**, **D2**, and **D3**.

Devices[a]	Turn-on voltage (V)	Luminance (cd/m)	Power efficiency (lm/W)	External quantum efficiency (%)	Luminance efficiency (cd/A)
D1	4.6	1180 (12160)[b]	3.70	2.47	11.80
D2	3.2	2060 (10800)[b]	6.12	4.42	20.60
D3	3.4	1010 (1770) [b]	2.21	1.84	10.10

[a] At 10 mA/cm.
[b] At 100 mA/cm.

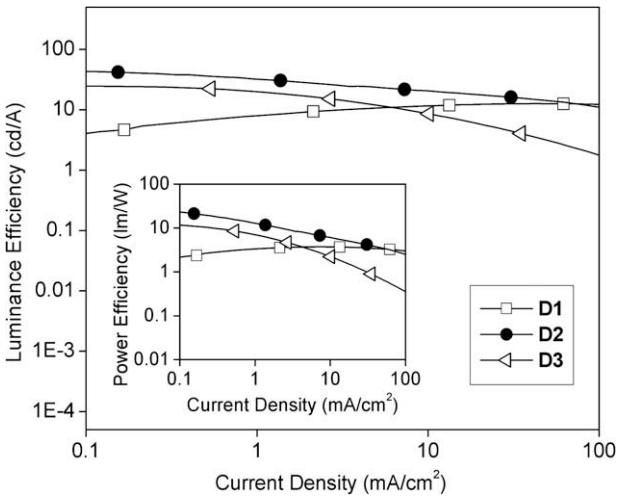

Fig. 7. Luminance efficiency vs. current density characteristics of devices **D1**, **D2**, and **D3**. Inset: Power efficiency vs. current density characteristics of the devices.

(Fig. 6). For example, at the current density of 10 mA/cm^2, the luminance of 2060 cd/m^2 for **D2** is almost two times higher than that for **D1** (1180 cd/m^2). Furthermore, according to the power and luminance efficiency vs. J plots for the devices shown in Fig. 7, the higher efficiency is consistently observed for **D2** in a wide range of current densities compared to that for **D1**. The efficiency values of 6.12 lm/W and 20.60 cd/A at 10 mA/cm for **D2** are much greater than those for **D1** (3.70 lm/W and 11.80 cd/A). In conjunction with higher external quantum efficiency, these results indicate that the device containing compound **2** as a hole-blocking material displays better device performances than the device based on BAlq HTL materials. On the other hand, in the case of **D3**, while the overall performances in terms of luminance, power and luminance efficiency, and external quantum efficiency are superior to those of **D1** in a relatively low current density range (below 10 mA/cm^2), they become lower in a high current density region. This result appears to be mainly involved with low thermal stability of **3** that may lead to lowering of device performance under high electrical bias stress. Despite the good performances of **D2** and **D3** devices, however, both devices showed the short device lifetime of within an hour for **D2** and several minutes for **D3** in comparison with that of the BAlq device (ca. 300 h). The short lifetime is likely to be related to the low thermal stability of **D2** and **D3** mainly caused by the low T_{d5} of **2** and **3**. Overall, all these results suggest that the four-coordinate boron compounds possessing [*N*,*O*] chelated 2-(2-pyridyl)phenol ligand may hold promise as a new kind of HBL materials in phosphorescent OLEDs once high thermal stability is achieved.

3. Conclusion

We have demonstrated that 2-(2-pyridyl)phenol (**1** · H) ligand can lead to the four-coordinate boron compounds of $Ph_2B \cdot$ **1** (**2**) and $(C_6F_5)_3B$(**1** · H) (**3**) via mono- or bidentate chelation to the boron atom depending on triarylborane starting materials. It was found that such boron compounds exhibit the ligand-centered, HOMO–LUMO electronic transitions and function as hole-blocking materials for phosphorescent OLEDs. Particularly, the device incorporating the bidentate [*N*,*O*] chelated system **2** as HBL materials displayed not only stable green phosphorescence of Ir(ppy)$_3$, but also high device performances in terms of luminance, power and luminance efficiency, and external quantum efficiency in a wide range of current densities.

Table 3
Crystallographic data and parameters for compounds **2** and **3**.

Compound	**2**	**3**
Empirical formula	$C_{23}H_{18}BNO$	$C_{29}H_9BF_{15}NO$ (1.5C_6H_6)
Formula weight	335.19	800.34
Temperature (K)	293(2)	296(2)
Crystal system	Triclinic	Monoclinic
Space group	$P\bar{1}$	$C2/c$
a (Å)	9.4401(14)	18.0034(9)
b (Å)	12.9483(18)	17.4323(8)
c (Å)	15.101(2)	22.9747(11)
α (°)	87.827(3)	90
β (°)	85.494(3)	100.041(3)
γ (°)	79.505(3)	90
V (Å^3)	1808.8(5)	7100.0(6)
Z	4	8
ρ_{calcd} (g/cm)	1.231	1.497
Wavelength (Å)	0.71073	0.71073
μ (nm^{-1})	0.074	0.144
F(000)	704	3208
2θ	1.60 – 28.08	1.64–24.58
hkl range	−12→8	−20→21
	−16→12	−19→20
	−19→19	−26→26
Number of reflections measured	11 325	25 063
Number of reflections used [R_{int}]	7860 [0.0240]	5913 [0.0354]
Refined parameters	469	506
Goodness-of-fit on F^2	1.005	1.001
R_1[a], wR_2[b] [$I > 2\sigma(I)$],	0.0438, 0.0664	0.0419, 0.0885
R_1[a], wR_2[b] [all data]	0.1293, 0.0761	0.0991, 0.1174
ρ_{fin} (max/min) (e/Å)	0.144/−0.171	0.135/−0.206

[a] $R_1 = \sum ||F_o| - |F_c|| / \sum |F_o|$.
[b] $wR_2 = [\sum[w(F_o^2 - F_c^2)^2] / \sum[w(F_o^2)^2]]^{1/2}$, where $w = 1/[\sigma^2(F_o^2) + (xP)^2 + yP]$, $P = (F_o^2 + 2F_c^2)/3$.

4. Experimental

4.1. General considerations

All operations were performed under inert nitrogen gas by using standard Schlenk and glovebox techniques. Anhydrous grade THF, CH_2Cl_2, and *n*-hexane (Aldrich) were purified by passing through an activated alumina column. Chemicals were used as received from Aldrich. 2-(2-pyridyl)phenol (**1** · H) was synthesized according to the reported procedure [11]. ^{1}H, ^{13}C, and ^{11}B NMR spectra were recorded on a Bruker Spectrospin 400 or a Bruker AM 300 spectrometer (400.13 MHz for ^{1}H, 100.62 MHz for ^{13}C, 96.28 MHz for ^{11}B) at ambient temperature. ^{19}F NMR spectra were recorded on a Bruker DRX300 spectrometer (282.38 MHz for ^{19}F) at Korea Basic Science Institute. Chemical shifts are given in ppm, and ^{1}H and ^{13}C NMR are referenced to the residual Me_4Si resonances. ^{19}F and ^{11}B chemical shifts are reported relative to $CFCl_3$ and $BF_3{\cdot}OEt_2$, respectively. Elemental analyses for C, H, and N were carried out on EA 1110-FISONS (CE Instruments) by the Environmental Analysis Laboratory at KAIST. Thermogravimetric analyses (TGA) were carried out under a nitrogen atmosphere at a heating rate of 10 °C/min with Dupont 9900 Analyzer. DSC measurements were carried out under a nitrogen atmosphere at a heating rate of

10 °C/min. UV–Vis and PL spectra were obtained on a Jasco V-530 and a Spex Fluorog-3 Luminescence spectrophotometer, respectively. Oxidation potentials of the compounds were determined by cyclic voltammetry (PAR273A) with a three-electrode cell configuration consisting of an ITO working electrode, a Pt counter electrode, and a $Ag/AgNO_3$ (0.1 M in acetonitrile) reference electrode at room temperature in CH_2Cl_2. The 0.1 M tetrabutylammonium hexafluorophosphate ($[n\text{-}Bu_4N][PF_6]$) was used as the supporting electrolyte. The oxidation potentials were recorded at a scan rate of 100 mV/s and reported with reference to the ferrocene/ferrocenium (Fc/Fc^+) redox couple.

4.2. Diphenylborinic acid 2-(2-pyridyl)phenol ester (**2**)

Triphenylborane (4 mL, 0.25 M in THF, 1 mmol) was added to a 50 mL of THF solution of **1** · H (0.17 g, 1 mmol). After refluxing for 6 h, the reaction mixture was cooled to ambient temperature. The solvent was removed in vacuo and the resulting solid was recrystallized from CH_2Cl_2/*n*-hexane (0.23 g, 70%). Single crystals suitable for X-ray structural determination were obtained by slow diffusion of *n*-hexane into a CH_2Cl_2 solution of **2**. For the EL measurements, **2** was further purified by sublimation at 180 °C. M.p.: 200 °C. ^{1}H NMR ($CDCl_3$, 400 MHz, ppm): δ = 6.81 (1H, m), 7.18–7.27 (12H, m), 7.36 (1H, m), 7.56 (1H, m), 7.89–7.93 (2H, m), 8.11 (1H, m); $^{13}C\{^1H\}$ NMR ($CDCl_3$, 100 MHz, ppm): δ = 118.38, 119.28, 120.62, 121.10, 121.72, 125.40, 126.42, 127.25, 133.25, 134.18, 140.59, 143.97, 148(br), 150.85, 160.06; $^{11}B\{^1H\}$ NMR ($CDCl_3$, 96.28 MHz, ppm): δ = 5.7; Anal. Calc. for $C_{23}H_{18}BNO$: C, 82.41; H, 5.41; N, 4.18. Found: C, 82.23; H, 5.44; N, 4.34%.

4.3. 2-(2-Pyridinium)phenolyl tris(pentafluorophenyl)borate (**3**)

Compound **3** was analogously prepared according to the above method using $B(C_6F_5)_3$ and **1** · H (1 mmol). Yield = 0.29 g (42%). Colorless single crystals suitable for X-ray structural determination were obtained by vapor diffusion of *n*-hexane into a benzene solution of **3**. M.p.: 160 °C. ^{1}H NMR ($CDCl_3$, 400 MHz, ppm): δ = 6.89–6.97 (2H, m), 7.32 (1H, m), 7.66 (1H, m), 7.78 (1H, m), 8.01 (1H, m), 8.30 (1H, m), 8.38 (1H, m), 16.63 (1H, s); $^{13}C\{^1H\}$ NMR ($CDCl_3$, 100 MHz, ppm): δ = 114.71, 120.21, 121(br), 122.65, 123.15, 127.58, 135.04, 136.86 (d, $^1J_{C-F}$ = 242 Hz), 136.90, 138.07, 139.38 (d, $^1J_{C-F}$ = 261 Hz), 144.87, 147.75 (d, $^1J_{C-F}$ = 241 Hz), 153.40, 159.77; $^{11}B\{^1H\}$ NMR ($CDCl_3$, 96.28 MHz, ppm): δ = −2.4; $^{19}F\{^1H\}$ NMR ($CDCl_3$, 282.38 MHz, ppm): δ = −135.1 (*o*-F), −159.1 (*p*-F), −164.8 (*m*-F); Anal. Calc. for $C_{29}H_9F_{15}BNO$: C, 50.98; H, 1.33; N, 2.05. Found: C, 50.56; H, 1.22; N, 2.01%.

4.4. X-ray structural determination

Single crystals of suitable size and quality were selected and mounted onto a glass capillary after coated with paraton oil. Reflection data were collected on a Bruker 1 K SMART CCD-area detector diffractometer with graphite-monochromated Mo Kα radiation (λ = 0.71073 Å). The hemisphere of reflection data were collected as ω-scan frames with a width of 0.3°/frame and exposure time of 10 s/frame. Cell parameters were determined and refined by SMART program [25]. Data reductions were performed using SAINT software [25], which corrects for Lorentz polarization effects, but any corrections for crystal decay were not required. Empirical absorption corrections were applied with SADABS program [26]. The structure was solved by direct methods and refined by full-matrix least-squares methods using the SHELXTL program package with anisotropic thermal parameters for all non-hydrogen atoms. Hydrogen atoms were placed at their geometrically calculated positions and refined riding on the corresponding carbon atoms with isotropic thermal parameters. The detailed crystallographic data and parameters for **2** and **3** are given in Table 3.

4.5. Computational details

The structure of **2** was optimized using the density functional theory (DFT) method with the B3LYP [22] functional and the 6-31G(d) [23] basis sets. Time-dependent density functional theory (TD-DFT) [27] using the hybrid B3LYP functional (TD-B3LYP) was used to obtain the electronic transition energies. To include the solvation effects of chloroform, the polarized continuum model (PCM) [24] was used in the calculations. All calculations described here were carried out using the GAUSSIAN 03 program [28].

4.6. Fabrication of OLEDs

OLEDs were fabricated by vacuum evaporation method under high vacuum. CuPc, α-NPD, CBP:$Ir(ppy)_3$ (8 wt%), **2** and **3** or BAlq, Alq_3, LiF, and Al were successively deposited on the pre-cleaned indium tin oxide-coated glass with the deposition rates of ca. 1 or 2 Å/s in a dry box. EL spectra were obtained with Ocean Optics USB2000 fiber-optic spectrometer. Current–voltage–luminance characteristics were recorded on Keithley 237 and Minolta CS-100A. EL measurements were carried out at room temperature under ambient atmosphere. The device lifetime was measured at the current density of 10 mA/cm^2 until the luminance decreases to half of the initial value.

Acknowledgment

Financial support from the Korea Science and Engineering Foundation (R01-2007-000-20299-0) and the BK 21 project is gratefully acknowledged. We would like to thank Dongwoo Fine-Chem Co. for assisting with the EL measurements and Dr. H. Kim for helping in computation.

Appendix A. Supplementary material

CCDC 705400 and 714877 contain the supplementary crystallographic data for this paper. These data can be obtained free of charge from The Cambridge Crystallographic Data Centre via www.ccdc.cam.ac.uk/data_request/cif. Supplementary data associated with this article can be found, in the online version, at doi:10.1016/j.jorganchem.2009.01.035.

References

[1] (a) M.A. Baldo, D.F. O'Brien, Y. You, A. Shoustikov, S. Sibley, M.E. Thompson, S.R. Forrest, Nature 395 (1998) 151;
(b) M.A. Baldo, D.F. O'Brien, M.E. Thompson, S.R. Forrest, Phys. Rev. B 60 (1999) 14422;
(c) C. Adachi, M.A. Baldo, M.E. Thompson, S.R. Forrest, J. Appl. Phys. 90 (2001) 5048;
(d) H. Yersin, Top. Curr. Chem. 241 (2004) 1;
(e) W.-Y. Wong, C.-L. Ho, Z.-Q. Gao, B.-X. Mi, C.-H. Chen, K.-W. Cheah, Z. Lin, Angew. Chem., Int. Ed. 45 (2006) 7800;
(f) L. Chen, H. You, C. Yang, D. Ma, J. Qin, Chem. Commun. (2007) 1352;
(g) P.-T. Chou, Y. Chi, Chem. -Eur. J. 13 (2007) 380.
[2] (a) D.F. O'Brien, M.A. Baldo, M.E. Thompson, S.R. Forrest, Appl. Phys. Lett. 74 (1999) 442;
(b) M. Ika, S. Tokito, Y. Sakamoto, T. Suzuki, Y. Taga, Appl. Phys. Lett. 79 (2001) 156;
(c) Y. Wang, N. Herron, V.V. Grushin, D. LeCloux, V. Petrov, Appl. Phys. Lett. 79 (2001) 449;
(d) K. Ono, T. Yanase, M. Ohkita, K. Saito, Y. Matsushita, S. Naka, H. Okada, H. Onnagawa, Chem. Lett. 33 (2004) 276.
[3] M.A. Baldo, S. Lamansky, P.E. Burrows, M.E. Thompson, S.R. Forrest, Appl. Phys. Lett. 75 (1999) 4.
[4] (a) Y. Kijima, N. Asai, S. Tamura, Jpn. J. Appl. Phys. 38 (1999) 5274;
(b) H.W. Lee, J.-G. An, H.-K. Yoon, H. Jang, N.G. Kim, Y. Do, Bull. Korean Chem. Soc. 13 (2001) 1167.

[5] R.C. Kwong, M.R. Nugent, L. Michalski, T. Ngo, K. Rajan, Y.-J. Tung, M.S. Weaver, T.X. Zhou, M. Hack, M.E. Thompson, S.R. Forrest, J.J. Brown, Appl. Phys. Lett. 81 (2002) 162.
[6] (a) T. Tsutschi, E. Aminaka, H. Tokuhisa, Synth. Met. 85 (1997) 1201;
(b) R. Fink, Y. Heischkel, M. Thelakkat, H.-W. Schmidt, Chem. Mater. 10 (1998) 3620;
(c) C. Wang, G.-Y. Jung, Y. Hua, C. Pearson, M.R. Bryce, M.C. Petty, A.S. Batsanov, A.E. Goeta, J.A.K. Howard, Chem. Mater. 13 (2001) 1167.
[7] C. Adachi, R. Kwong, P. Djurovich, V. Adamovich, M.A. Baldo, M.E. Thompson, S.R. Forrest, Appl. Phys. Lett. 79 (2001) 2082.
[8] (a) K. Okumoto, Y. Shirota, Chem. Mater. 15 (2003) 699;
(b) M. Kinoshita, H. Kita, Y. Shirota, Adv. Funct. Mater. 12 (2002) 780.
[9] K.Y. Hwang, M.H. Lee, H. Jang, Y. Sung, J.S. Lee, S.H. Kim, Y. Do, Dalton Trans. (2008) 1818.
[10] (a) Q. Wu, M. Esteghamatian, N.-X. Hu, Z. Popovic, G. Enright, Y. Tao, M. D'Iorio, S. Wang, Chem. Mater. 12 (2000) 79;
(b) Y. Qin, C. Pagba, P. Piotrowiak, F. Jäkle, J. Am. Chem. Soc. 126 (2004) 7015;
(c) Y. Cui, Q.-D. Liu, D.-R. Bai, W.-L. Jia, Y. Tao, S. Wang, Inorg. Chem. 44 (2005) 601;
(d) S. Anderson, M.S. Mudadu, R. Thummel, Y. Tao, S. Wang, Adv. Funct. Mater. 15 (2005) 143;
(e) S. Wang, Coord. Chem. Rev. 215 (2001) 79;
(f) S.-F. Liu, C. Seward, H. Aziz, N.-X. Hu, Z. Popovic, S. Wang, Organometallics 19 (2000) 5709;
(g) Q.-D. Liu, M.S. Mudadu, R. Thummel, Y. Tao, S. Wang, Adv. Funct. Mater. 15 (2005) 143;
(h) Q.-D. Liu, M.S. Mudadu, H. Schmider, R. Thummel, Y. Tao, S. Wang, Organometallics 21 (2002) 4743.
[11] Y.L. Teng, Y.H. Kan, Z.M. Su, Y. Liao, S.Y. Yang, R.S. Wang, Theor. Chem. Acc. 117 (2007) 1.
[12] L. Kaczmarek, R. Balicki, J. Lipkowski, P. Borowicz, A. Grabowska, J. Chem. Soc. Perkin Trans. 27 (1994) 1603.
[13] (a) Y. Liu, J. Guo, J. Feng, H. Zhang, Y. Li, Y. Wang, Appl. Phys. Lett. 78 (2001) 2300;
(b) Z.Y. Xie, J.S. Huang, C.N. Li, S.Y. Liu, Y. Wang, Y.Q. Li, J.C. Shen, Appl. Phys. Lett. 74 (1999) 641;
(c) W.S. Jeon, T.J. Park, J.J. Park, S.Y. Kim, J. Jang, J.H. Kwon, R. Pode, Appl. Phys. Lett. 92 (2008) 113311.
[14] Y. Li, Y. Liu, W. Bu, D. Lu, Y. Wu, Y. Wang, Chem. Mater. 12 (2000) 2672.
[15] (a) H. Murata, H. Nakashima, S. Kawakami, N. Ohsawa, R. Nomura, S. Seo, US Pat. Appl. Publ. US 2007149784, 2007.;
(b) R. Kwong, Y.-J. Tung, B. Ma, D.B. Knowles, US Pat. Appl. Publ. US 2005019605, 2005.;
(c) T. Enokida, S. Okutsu, M. Tamano, Jpn. Kokai Tokkyo Koho JP 09176629, 1997.;
(d) D.Y. Kondakov, T.L. Royster, C.T. Brown, US Pat. Appl. Publ. US 2007134514, 2007.;
(e) H. Tanaka, M. Mohri, H. Takeuchi, O. Watanabe, T. Mori, S. Tokito, Jpn. Kokai Tokkyo Koho JP 2000357588, 2000.
[16] (a) H. Tanaka, S. Tokito, Y. Taga, A. Okada, J. Mater. Chem. 8 (1998) 1999;
(b) S. Tokito, K. Noda, H. Tanaka, Y. Taga, T. Tsutsui, Synth. Met. 111–112 (2000) 393.
[17] J. Ugolotti, S. Hellstrom, G.J.P. Britovsek, T.S. Jones, P. Hunt, A.J.P. White, Dalton Trans. (2007) 1425.
[18] H. Höpfl, V. Barba, G. Vargas, N. Farfan, R. Santillan, D. Castillo, Chem. Heterocycl. Compd. 35 (1999) 912.
[19] Y. Liao, Y.G. Chen, Z.M. Su, Y.H. Kan, H.X. Duan, D.X. Zhu, Synth. Met. 137 (2003) 1093.
[20] (a) W.L. Jia, X.D. Feng, D.R. Bai, Z.H. Lu, S. Wang, G. Vamvounis, Chem. Mater. 17 (2005) 164;
(b) J.-U. Kim, H.-B. Lee, J.-S. Shin, Y.-H. Kim, Y.-K. Joe, H.-Y. Oh, C.-G. Park, S.-K. Kwon, Synth. Met. 150 (2005) 27.
[21] W.H. Melhuish, J. Phys. Chem. 65 (1961) 229.
[22] P.J. Stephens, F.J. Devlin, C.F. Chabalowski, M.J. Frisch, J. Phys. Chem. 98 (1994) 11623.
[23] J.S. Binkley, J.A. Pople, W.J. Hehre, J. Am. Chem. Soc. 102 (1980) 939.
[24] (a) S. Miertus, E. Scrocco, J. Tomasi, J. Chem. Phys. 55 (1981) 117;
(b) R. Cammi, J. Tomasi, J. Comput. Chem. 16 (1995) 1449;
(c) B. Mennucci, J. Tomasi, R. Cammi, J.R. Cheeseman, M.J. Frisch, F.J. Devlin, S. Gabriel, P.J. Stephens, J. Phys. Chem. A 106 (2002) 6102.
[25] SMART, Version 5.0, Data collection software, Bruker AXS Inc., USA, 1998.
[26] G.M. Sheldrick, SADABS, Program for Absorption Correction with the Bruker SMART System, Universität Göttingen, Germany, 1996.
[27] E. Runge, E.K. Gross, Phys. Rev. Lett. 52 (1984) 997.
[28] GAUSSIAN 03, Revision C.02, M.J. Frisch, et al., Gaussian Inc., Wallingford CT, 2004.